Electron paramagnetic resonance and electron-nuclear double resonance study of the neutral copper acceptor in $ZnGeP_2$ crystals

2003 J. Phys.: Condens. Matter 15 1625

(http://iopscience.iop.org/0953-8984/15/10/311)

INSTITUTE OF PHYSICS PUBLISHING JOURNAL OF PHYSICS: CONDENSED MATTER

J. Phys.: Condens. Matter **15** (2003) 1625–1633 PII: S0953-8984(03)52299-8

Electron paramagnetic resonance and electron-nuclear double resonance study of the neutral copper acceptor in $ZnGeP_2$ crystals

K T Stevens[1,3], L E Halliburton[1,4], S D Setzler[2], P G Schunemann[2] and T M Pollak[2]

[1] Department of Physics, West Virginia University, Morgantown, WV 26506, USA
[2] BAE Systems, Nashua, NH 03061, USA

E-mail: Larry.Halliburton@mailwvu.edu

Received 13 August 2002, in final form 9 January 2003
Published 3 March 2003
Online at stacks.iop.org/JPhysCM/15/1625

Abstract

Electron paramagnetic resonance (EPR) and electron-nuclear double resonance have been used to characterize the neutral copper acceptor in $ZnGeP_2$ crystals. The copper substitutes for zinc and behaves as a conventional acceptor (i.e. the 3d electrons do not play a dominant role). Because of a high degree of compensation from native donors, the copper acceptors in our samples were initially in the nonparamagnetic singly ionized state (Cu^{-}_{Zn}). The paramagnetic neutral state (Cu^{0}_{Zn}) was observed when the crystals were exposed to 632.8 nm or 1064 nm laser light while being held at a temperature below 50 K. The g matrix of the neutral copper acceptor is axial ($g_{\parallel} = 2.049$ and $g_{\perp} = 2.030$), with the unique principal direction parallel to the tetragonal c axis of the crystal. The hyperfine and nuclear quadrupole matrices also exhibit c-axis symmetry ($A_{\parallel} = 87.6$ MHz, $A_{\perp} = 34.8$ MHz and $P = 0.87$ MHz for ^{63}Cu and $A_{\parallel} = 93.9$ MHz, $A_{\perp} = 37.3$ MHz and $P = 0.81$ MHz for ^{65}Cu). Equal hyperfine interactions with the four nearest-neighbour phosphorus ions are well resolved in the c-axis EPR spectrum.

1. Introduction

Zinc germanium phosphide ($ZnGeP_2$) is a semiconductor from the ternary chalcopyrite family of materials [1, 2]. The II–IV–V_2 chalcopyrites are analogous to the widely studied III–V materials GaP and GaAs, except that their crystal structure is tetragonally distorted from the simpler zinc-blende structure of the III–V compounds. In particular, GaP is converted to $ZnGeP_2$ by replacing, in an alternating sequence, half of the Ga ions with Zn and half with Ge.

[3] Present address: Northrop Grumman Space Technology, Synoptics, Charlotte, NC 28273, USA.
[4] Author to whom any correspondence should be addressed.

The space group for the ternary chalcopyrites is $I\bar{4}2d$ and the point group is $\bar{4}2m$. Excellent nonlinear optical properties make $ZnGeP_2$ a preferred material for optical parametric oscillator (OPO) applications in the mid-infrared [3–6]. This material is also a viable candidate for future spintronic devices because of its ferromagnetic behaviour at room temperature when heavily doped with Mn [7–9]. At the present time, however, many of the optical and electrical properties of $ZnGeP_2$ crystals are dominated by intrinsic donors and acceptors (i.e. vacancies and antisites) introduced unintentionally during growth. Further development of $ZnGeP_2$ for both infrared frequency conversion and spintronic applications depends upon the ability to minimize these native defects and, in turn, achieve controlled n- and p-type behaviour through doping.

Electron paramagnetic resonance (EPR) and electron-nuclear double resonance (ENDOR) have proven to be effective techniques for identifying point defects in single crystals of $ZnGeP_2$. Thus far, defect assignments have been made for three native donors and one native acceptor. A series of EPR and ENDOR studies [10–12] have suggested that the dominant acceptor in bulk $ZnGeP_2$ is the singly ionized zinc vacancy (the V_{Zn}^- centre). Photoinduced EPR studies [13, 14] have described the neutral phosphorus vacancy (the V_P^0 donor) and the singly ionized germanium-on-a-zinc antisite (the Ge_{Zn}^+ donor). An earlier EPR study described the photoinduced spectrum from a phosphorus antisite defect [15], presumably the neutral P_{Ge}^0 donor. The only impurity in $ZnGeP_2$ that has been studied with EPR is Mn^{2+} ($3d^5$) substituting for zinc [16, 17]. Other investigations have focused on the optical absorption and luminescence associated with native defects in $ZnGeP_2$ [18–24]. Also, the luminescence from a series of $ZnGeP_2$ crystals diffusion-doped with copper has been described [25].

In the present paper, we describe the results of an EPR and ENDOR study of copper impurities substituting for zinc in $ZnGeP_2$ crystals. The paramagnetic neutral state of copper (Cu_{Zn}^0) is photoinduced at low temperature, i.e. electrons are effectively pumped from the singly ionized Cu_{Zn}^- centres to donors where they remain for times on the order of minutes. The g matrix of the Cu_{Zn}^0 centre is only slightly anisotropic with principal values near 2.0, and there is significant overlap of the unpaired spin with the surrounding phosphorus ions. Together, these observations suggest that copper behaves as a conventional acceptor in $ZnGeP_2$. In the paramagnetic state, covalency effects result in the bound hole being less atomic-like and more effective-mass-like, thus reflecting the character of the host valence bands [26]. Before proceeding, it is useful to clarify the semiconductor notation being used. The Cu_{Zn}^0 label refers to a neutral copper atom that has replaced a neutral zinc atom in the lattice (this is an A^0 centre in semiconductor terms). The Cu_{Zn}^- label refers to copper that has accepted an extra electron (this is an A^- centre in semiconductor terms). The singly ionized Cu_{Zn}^0 acceptor and the neutral Cu_{Zn}^- acceptor both have the $3d^{10}$ configuration; they also have either one or two electrons, respectively, to participate in bonding with the four neighbouring phosphorus ions.

In general, copper impurities often play important roles in the optical and electrical properties of semiconductors (especially the II–VI compounds), and their associated EPR spectra are of particular interest because of the insight they provide about the electronic structure of the specific centres. As an example, copper substituting for zinc in wurtzite-structured ZnO has $g_\parallel = 0.74$ and $g_\perp = 1.531$, with the proposed explanation of these large g shifts being a significant delocalization of the 3d hole onto the nearest-neighbour oxygen ions [27]. Also, in many semiconductors, there is a tendency for copper to form complex centres by associating with other defects (i.e. vacancies and/or interstitials). A large number of these copper complexes have been detected [28] with EPR in ZnS. And, in GaP, optically detected magnetic resonance (ODMR) has been used to characterize a copper-related neutral complex [29]. Thus far, there have been no reports of EPR spectra from isolated copper acceptors in ZnS, ZnSe, ZnTe, CdTe and GaP. This lack of previous EPR results describing the isolated neutral copper acceptor gives added importance to our present investigation.

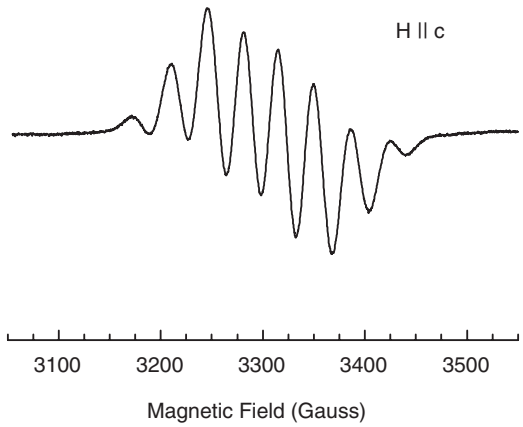

Figure 1. Photoinduced EPR spectrum of the neutral Cu^0_{Zn} acceptor in $ZnGeP_2$. The sample temperature was 12 K, the magnetic field was parallel to the *c* axis and the microwave frequency was 9.441 GHz.

2. Experimental details

The $ZnGeP_2$ crystals used in this investigation were grown by the horizontal gradient freeze technique at BAE Systems in Nashua, NH (formerly known as Sanders, a Lockheed Martin Company). These crystals contained at least 3 ppm of copper, as estimated from the intensity of the EPR Cu^0_{Zn} signal. This is a lower limit for the copper concentration since not all of the copper may be present as isolated centres and not all of the isolated copper may be converted to neutral acceptors. Typical sample dimensions were $2 \times 3 \times 5$ mm^3, with edges parallel to the [100], [010] and [001] directions. These crystal directions are referred to as the *a*, *b* and *c* axes, respectively, where *a* and *b* are equivalent axes and *c* is the unique axis. A Bruker ESP 300 spectrometer operating near 9.44 GHz was used to obtain the EPR and ENDOR data. For the EPR experiments, a rectangular Bruker microwave cavity was used with 100 kHz modulation of the magnetic field. The microwave frequency was measured with a Hewlett-Packard 5340A counter and the static magnetic field was measured with a Varian E-500 proton gaussmeter. A small MgO:Cr crystal was used to correct for the difference in magnetic field between the sample and the gaussmeter probe (the isotropic *g* value for Cr^{3+} in MgO is 1.9800). A cylindrical Bruker cavity was used in the ENDOR experiments; the coil was placed inside the cavity and the rf was frequency modulated at 12.5 kHz. Temperatures were maintained with helium-gas flow systems (Oxford Instruments ESR-900) extending through the microwave cavities. The neutral Cu^0_{Zn} centres were formed at low temperature using a helium–neon laser (632.8 nm) or a Nd:YAG laser (1064 nm). Slots in the end of the EPR cavity provided easy optical access to the crystal. The ENDOR cavity did not have slots, so a small optical fibre attached alongside the sample support rod was used to guide the laser beam to the crystal.

3. Results

The EPR spectrum of the photoinduced Cu^0_{Zn} centre in $ZnGeP_2$ is shown in figure 1. These data were taken at 12 K during continuous 632.8 nm laser excitation and with the magnetic field parallel to the *c* axis of the crystal. Even though a large concentration of zinc-vacancy acceptors (V^-_{Zn} centres) are present in the crystal, their EPR spectrum [10] is strongly saturated with microwave power at 12 K and they are not visible in figure 1. Photoinduced donor

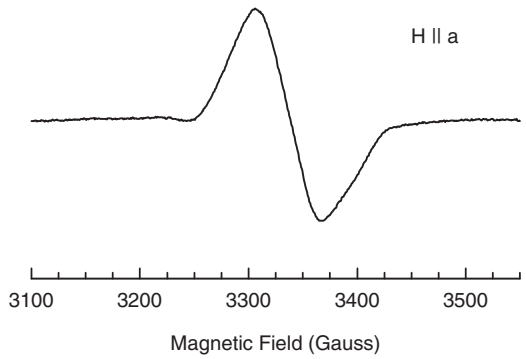

Figure 2. Photoinduced EPR spectrum of the neutral Cu^0_{Zn} acceptor taken with the magnetic field parallel to the *a* axis. The sample temperature was 12 K and the microwave frequency was 9.442 GHz.

signals [13, 14] from the phosphorus vacancy (V_P^0) and the germanium-on-a-zinc antisite (Ge^+_{Zn}) are also present in the sample, but are not observed in figure 1 because they have considerably larger EPR linewidths than the Cu^0_{Zn} centres (i.e. the smaller modulation amplitude employed in figure 1 favours the Cu^0_{Zn} centres). The Cu^0_{Zn} signal is best seen at low temperatures ($<$20 K) and high microwave powers. Although a 20 mW helium–neon laser (632.8 nm) was our primary source to produce the EPR signal, we found that a 1064 nm laser beam could also easily produce the signal. If the laser beam is removed from the sample, the Cu^0_{Zn} signal decays slowly over a period of tens of minutes at temperatures less than 20 K. We have found that this decay time is sample dependent and is controlled primarily by the specific donors that are present.

The *c*-axis Cu^0_{Zn} spectrum in figure 1 consists of eight lines; the four central lines have approximately equal intensities and two progressively weaker lines appear on each side of the four lines. This hyperfine pattern can be explained with one copper ion and four phosphorus ions. The two isotopes of copper, ^{63}Cu (69.2% abundant) and ^{65}Cu (30.8% abundant), both have $I = 3/2$ nuclear spins and give rise to the four centre lines. Their magnetic moments are similar, which explains why separate hyperfine patterns are not resolved in figure 1 for the two isotopes. Each of the four centre lines is then split into five lines with a 1:4:6:4:1 intensity ratio as a result of approximately equal hyperfine interactions with the four neighbouring phosphorus nuclei (^{31}P, 100% abundant, $I = 1/2$). This gives a large number of lines contributing to the *c*-axis EPR spectrum, but many of them are overlapping. Only eight 'apparent' lines are observed because the magnitudes of the copper and phosphorus hyperfine interactions are similar for this orientation of the magnetic field.

The EPR spectrum from the neutral Cu^0_{Zn} acceptor reduces to a single broad line with no resolvable hyperfine structure when the magnetic field is oriented perpendicular to the *c* axis. This is shown in figure 2, where the data were taken at 12 K with the magnetic field along the *a* axis of the crystal. There were no shifts in line position or changes in line shape as the magnetic field was rotated 90° from the *a* axis to the *b* axis in the basal plane. This strongly suggests that the *g* matrix and the ^{63,65}Cu hyperfine matrices are axial with their unique principal directions parallel to the *c* axis of the crystal (i.e. the axis of tetragonal symmetry). From EPR measurements along the *c* and *a* axes, we determined that $g_\parallel = 2.049$ and $g_\perp = 2.030$. Error limits for these *g* values are approximately ± 0.003.

Additional information about the neutral Cu^0_{Zn} acceptor in $ZnGeP_2$ was obtained using ENDOR. The EPR signal did not easily saturate with microwave power, thus relaxation

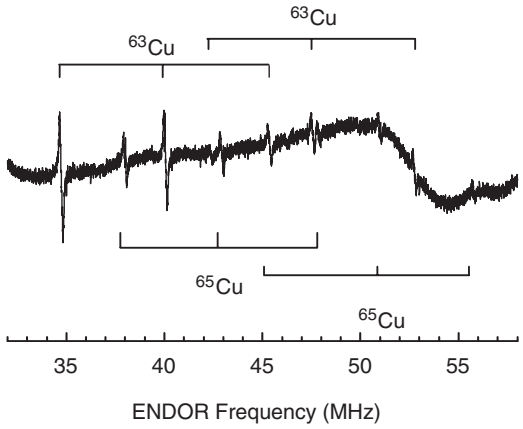

Figure 3. Photoinduced ENDOR spectrum of the neutral Cu^0_{Zn} acceptor in $ZnGeP_2$. The data were taken at 12 K with the magnetic field (3290.0 G) parallel to the *c* axis.

conditions were not optimum for ENDOR measurements. Also, the intensity of the excitation light at the sample was reduced as a result of using an optical fibre to transmit the laser beam into the cavity, and this made acquiring the ENDOR data more difficult due to a less intense EPR signal. Nevertheless, ENDOR spectra associated with ^{63}Cu, ^{65}Cu and ^{31}P nuclei were obtained with the magnetic field along the *c* and *a* crystal axes. The ENDOR spectrum shown in figure 3 was taken at 12 K with the magnetic field along the *c* axis. Transitions from both copper isotopes can be seen, thus verifying that copper is indeed the cause of the four central lines in the *c*-axis EPR spectrum (see figure 1). The hyperfine constant, A, for each isotope is larger than the corresponding free nuclear resonance frequency, ν_N, and there are significant nuclear quadrupole splittings. Two sets of three lines are assigned to each copper isotope and, to a first approximation, the two middle lines for a specific isotope are centred on $A/2$ and separated by $2\nu_N$.

The stick diagrams in figure 3 show the isotope assignments for each of the copper ENDOR lines (these data were taken at a magnetic field of 3290.0 G). For ^{63}Cu, the middle lines of each set are centred on 43.8 MHz and are separated by 7.51 MHz. The expected value of $2\nu_N$ for ^{63}Cu, obtained from tables of known g_N values [30], is 7.45 MHz. This agreement between the expected value of $2\nu_N$ and the experimental separation is quite reasonable. For ^{65}Cu, the middle lines of each set are centred on 47.0 MHz and are separated by 8.04 MHz. The expected value of $2\nu_N$ for ^{65}Cu is 7.97 MHz (when the magnetic field is 3290.0 G). Our experimental separation of the middle lines for ^{65}Cu compares favourably with this expected value. Also, we note that the ratio of the experimentally determined centre positions for the middle lines of the ^{63}Cu and ^{65}Cu sets is in good agreement with the known ratio of the nuclear magnetic moments for the two copper isotopes (i.e. 0.932 for the ratio of centre frequencies and 0.935 for the ratio of magnetic moments).

The *a*-axis ENDOR spectrum of the Cu^0_{Zn} acceptor, showing the transitions associated with the copper isotopes, is presented in figure 4. There is a significant increase in the signal-to-noise ratio for the spectrum in figure 4, compared to figure 3, which suggests that the relaxation conditions for ENDOR are more favourable when the magnetic field is along the *a* axis of the crystal. Stick diagrams designate the ENDOR transitions for both ^{63}Cu and ^{65}Cu. The ENDOR signals have shifted to lower frequencies and the two sets of three lines for a given isotope are no longer overlapping, thus indicating the hyperfine and quadrupole interactions are both

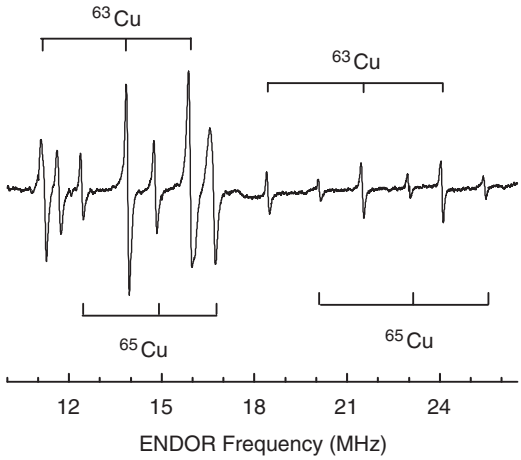

Figure 4. Photoinduced ENDOR spectrum of the neutral Cu^0_{Zn} acceptor. The sample temperature was 12 K and the magnetic field (3329.8 G) was parallel to the *a* axis.

smaller for this orientation of magnetic field. Even though the copper hyperfine interaction is smaller in figure 4, the ENDOR lines are still centred, to first order, on A/2 and split by $2\nu_N$. Also, it is important to note that there are no site splittings in this *a*-axis spectrum. As the magnetic field was rotated away from the *a* axis toward the [110] direction, the ENDOR spectra quickly became very weak and then unobservable after a rotation of only 10°. This lack of ENDOR data at a variety of angles in the basal plane prevented us from demonstrating directly that the hyperfine and nuclear quadrupole interactions for the copper nuclei were axial. It is, nonetheless, a reasonable approximation to treat these interactions as axial (and thus reflecting the symmetry of the unperturbed lattice) since there was no variation in the EPR signal when the magnetic field was rotated in the basal plane and there was no site splitting in the *a*-axis ENDOR spectrum. Furthermore, the *c*-axis EPR spectrum (see figure 1) indicates that all four phosphorus ions are occupying their normal positions as nearest neighbours of the copper. A neighbouring defect, if present, must be at least several lattice spaces away from the copper acceptor.

The following spin Hamiltonian describes the EPR and the ^{63,65}Cu ENDOR spectra of the neutral Cu^0_{Zn} acceptor:

$$H = \beta \boldsymbol{S}\cdot\boldsymbol{g}\cdot\boldsymbol{B} + \boldsymbol{I}\cdot\boldsymbol{A}\cdot\boldsymbol{S} + \boldsymbol{I}\cdot\boldsymbol{Q}\cdot\boldsymbol{I} - g_n\beta_n\boldsymbol{I}\cdot\boldsymbol{B}.$$

We take the $\boldsymbol{g}$, $\boldsymbol{A}$ and $\boldsymbol{Q}$ matrices to be axial (with the unique direction of each matrix along the *c* axis of the crystal). In the case of the $\boldsymbol{Q}$ matrix, the diagonal elements are $Q_{xx} = -P$, $Q_{yy} = -P$ and $Q_{zz} = 2P$. The parameter P is defined as $e^2qQ/[4I(2I-1)]$, where eq is the electric field gradient and Q is the nuclear quadrupole moment. Using a least-squares computer fitting procedure, we determined the 'best' values of the hyperfine and quadrupole parameters. A set of 12 experimental ENDOR frequencies (six from the *c*-axis spectrum and six from the *a*-axis spectrum) was used to fit $A_\parallel$, $A_\perp$ and P for the ^{63}Cu isotope and a second set of twelve ENDOR frequencies (also from the *c*- and *a*-axes spectra) were used to fit $A_\parallel$, $A_\perp$ and P for the ^{65}Cu isotope. The best values for these parameters are given in table 1. Our experiments could not determine the absolute signs of these parameters. It is interesting to compare the ratio of our nuclear quadrupole parameters for the two isotopes of copper with the values of the nuclear quadrupole moments (−0.222 for ^{63}Cu and −0.195 for ^{65}Cu, in units of $|e| \times 10^{-24}$ cm^2) given in standard tables [30]. These 'standard' values

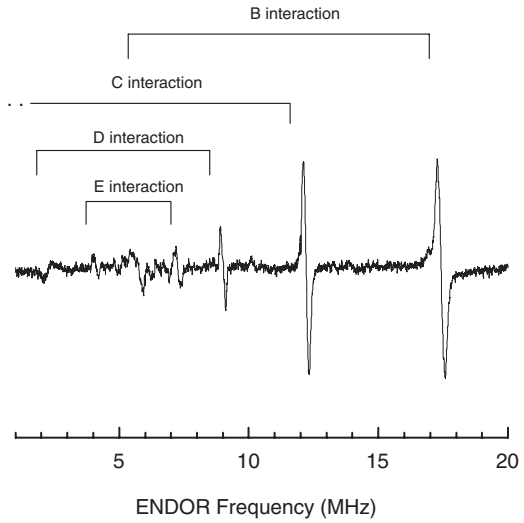

Figure 5. Phosphorus (^{31}P) ENDOR spectrum taken from the neutral copper acceptor. The sample temperature was 12 K and the magnetic field (3290.0 G) was parallel to the *c* axis. Note that the low-frequency line associated with the C interaction is near 0.5 MHz, and thus is out of the range of the ENDOR spectrometer.

Table 1. Hyperfine and nuclear quadrupole parameters for the neutral copper acceptor (Cu^0_{Zn}) in $ZnGeP_2$. Values are given for the ^{63}Cu and the ^{65}Cu isotopes. Estimated errors are ± 0.1 MHz for the hyperfine parameters and ± 0.005 MHz for the quadrupole parameter.

	$A_\parallel$ (MHz)	$A_\perp$ (MHz)	P (MHz)
^{63}Cu	87.6	34.8	0.87
^{65}Cu	93.9	37.3	0.81

give a ratio of 1.14, while our parameters in table 1 give a ratio of 1.07. We note that, in a separate ENDOR study of copper [31], the ratio of the three experimentally determined nuclear quadrupole principal values for the two isotopes were 1.05, 1.07 and 1.07. These latter values directly agree with our experimental ratio.

Hyperfine interactions with the neighbouring phosphorus nuclei were also present in the ENDOR spectra from the Cu^0_{Zn} acceptor. The *c*-axis EPR data in figure 1 suggested that the unpaired spin interacted nearly equally with four phosphorus ions, and we observed a set of very weak intensity ^{31}P ENDOR lines that supported this interpretation. This *c*-axis ENDOR spectrum, taken at 3290.0 G, consisted of two sets of lines (each set having three closely spaced components) centred on 54.7 MHz and split by 10.21 MHz. The corresponding value of $2\nu_N$ for the ^{31}P nucleus is 11.35 MHz, and this is close to the experimental separation of 10.21 MHz. We suggest that these two sets of closely spaced ENDOR lines are due to equivalent hyperfine interactions with multiple ^{31}P nuclei. The A/2 value of 54.7 MHz agrees well with the superhyperfine splitting of 39.1 G observed in figure 1. In addition to the strong interaction with the nearest-neighbour phosphorus ions (which is labelled the A interaction), we observed ENDOR lines at lower rf frequencies (with the magnetic field along the *c* axis) that represent weaker interactions with more distant phosphorus neighbours. These data are shown in figure 5. Four of these phosphorus interactions, labelled B, C, D and E, are easily recognized. The B and C pairs of ENDOR lines represent larger interactions and are centred on

Table 2. . Summary of the *c*-axis hyperfine values for phosphorus neighbours of the Cu^0_{Zn} acceptor in $ZnGeP_2$. Other than the A interaction, which corresponds to the nearest neighbours, they are not assigned to particular phosphorus sites surrounding the copper. Estimated errors are ±0.1 MHz for these parameters.

	c-axis hyperfine (MHz)
^{31}P (A interaction)	109.4
^{31}P (B interaction)	23.5
^{31}P (C interaction)	13.1
^{31}P (D interaction)	6.7
^{31}P (E interaction)	3.2

$A/2$ and split by $2\nu_N$, while the D and E pairs of ENDOR lines represent smaller interactions and are centred on ν_N and split by A. The *c*-axis hyperfine values for these interactions between the Cu^0_{Zn} acceptor and its phosphorus neighbours are listed in table 2.

4. Summary

In summary, we have observed a photoinduced paramagnetic centre in $ZnGeP_2$ which we assign to the neutral state of the copper acceptor (Cu^0_{Zn}). The copper substitutes for zinc and there are no perturbing defects nearby. The g matrix ($g_\parallel = 2.049$ and $g_\perp = 2.030$) and the ^{63,65}Cu hyperfine and nuclear quadrupole matrices have axial symmetry, with the unique direction of each matrix parallel to the c axis of the crystal. Principal g values near 2.0 and significant delocalization of the unpaired spin, as demonstrated by superhyperfine interactions with several shells of surrounding phosphorus ions, combine to suggest that the Cu^0_{Zn} centre is behaving as a conventional acceptor in $ZnGeP_2$. Following the approach of Robbins *et al* [26], this means that the effective d-orbital occupancy is minimal for the Cu^0_{Zn} acceptor in $ZnGeP_2$. Instead, the hole consists primarily of host valence band orbitals. Behaviour of this type has been expected for isolated neutral copper acceptors in ZnTe and CdTe, but has never before been experimentally verified with EPR. Future computational and experimental studies should lead to a better understanding of the copper acceptor in $ZnGeP_2$ and, more generally, in all zinc-based semiconductors.

Acknowledgments

This research was supported at West Virginia University by the Air Force Office of Scientific Research (grants F49620-99-1-0248 and F49620-01-1-0428) and by the National Science Foundation (grant DMR-9807128). The work at BAE Systems was supported by the Air Force Research Laboratory (Materials Directorate at WPAFB) under contract no F33615-94-C-5415.

References

[1] Shay J L and Wernick J H 1975 *Ternary Chalcopyrite Semiconductors: Growth, Electronic Properties, and Applications* (New York: Pergamon)
[2] Rud Yu V 1994 *Semiconductors* **28** 633 and references therein
[3] Barnes N P 1995 *Tunable Lasers Handbook* ed F J Duarte (New York: Academic) ch 7, pp 293–348
[4] Schunemann P G, Schepler K L and Budni P A 1998 *MRS Bull.* **23** 45
[5] Budni P A, Pomeranz L A, Lemons M L, Miller C A, Mosto J R and Chicklis E P 2000 *J. Opt. Soc. Am.* B **17** 723

[6] Vodopyanov K L, Ganikhanov F, Maffetone J P, Zwieback I and Ruderman W 2000 *Opt. Lett.* **25** 841
[7] Cho S, Choi S, Cha G, Hong S C, Kim Y, Zhao Y, Freeman A J, Ketterson J B, Kim B J, Kim Y C and Choi B 2002 *Phys. Rev. Lett.* **88** 257203
[8] Medvedkin G A, Hirose K, Ishibashi T, Nishi T, Voevodin V G and Sato K 2002 *J. Cryst. Growth* **236** 609
[9] Zhao Y, Picozzi S, Continenza A, Geng W T and Freeman A J 2002 *Phys. Rev.* B **65** 094415/1-6
[10] Rakowsky M H, Kuhn W K, Lauderdale W J, Halliburton L E, Edwards G J, Scripsick M P, Schunemann P G, Pollak T M, Ohmer M C and Hopkins F K 1994 *Appl. Phys. Lett.* **64** 1615
[11] Halliburton L E, Edwards G J, Scripsick M P, Rakowsky M H, Schunemann P G and Pollak T M 1995 *Appl. Phys. Lett.* **66** 2670
[12] Stevens K T, Setzler S D, Halliburton L E, Fernelius N C, Schunemann P G and Pollak T M 1998 *Mater. Res. Soc. Symp. Proc.* **484** 549
[13] Giles N C, Halliburton L E, Schunemann P G and Pollak T M 1995 *Appl. Phys. Lett.* **66** 1758
[14] Setzler S D, Giles N C, Halliburton L E, Schunemann P G and Pollak T M 1999 *Appl. Phys. Lett.* **74** 1218
[15] Kaufmann U, Schneider J and Rauber A 1976 *Appl. Phys. Lett.* **29** 312
[16] Baran N P, Tychina I I, Tregub I G, Tkachuk I Yu, Chernenko L I and Shcherbyna I P 1975 *Sov. Phys.–Semicond.* **9** 1527
[17] Setzler S D, Halliburton L E, Giles N C, Schunemann P G and Pollak T M 1997 *Mater. Res. Soc. Symp. Proc.* **450** 327
[18] Setzler S D, Schunemann P G, Pollak T M, Ohmer M C, Goldstein J T, Hopkins F K, Stevens K T, Halliburton L E and Giles N C 1999 *J. Appl. Phys.* **86** 6677
[19] Stevens K T, Setzler S D, Schunemann P G, Pollak T M, Giles N C and Halliburton L E 2000 *Mater. Res. Soc. Symp. Proc.* **607** 379
[20] Zwieback I, Maffetone J, Perlov D, Harper J, Ruderman W, Bachmann K and Dietz N 2000 *Mater. Res. Soc. Symp. Proc.* **607** 409
[21] Moldovan M, Stevens K T, Halliburton L E, Schunemann P G, Pollak T M, Setzler S D and Giles N C 2000 *Mater. Res. Soc. Symp. Proc.* **607** 445
[22] Moldovan M and Giles N C 2000 *J. Appl. Phys.* **87** 7310
[23] Rablau C I and Giles N C 2001 *J. Appl. Phys.* **90** 3314
[24] Gehlhoff W, Pereira R N, Azamat D, Hoffmann A and Dietz N 2001 *Physica* B **308–310** 1015
[25] Wang L, Bai L, Stevens K T, Garces N Y, Giles N C, Setzler S D, Schunemann P G and Pollak T M 2002 *J. Appl. Phys.* **92** 77
[26] Robbins D J, Dean P J, Simmonds P E and Tews H 1992 *Deep Centers in Semiconductors* 2nd edn, ed S T Pantelides (Yverdon: Gordon and Breach) ch 11, pp 843–98
[27] Dietz R E, Kamimura H, Sturge M D and Yariv A 1963 *Phys. Rev.* **132** 1559
[28] Holton W C, De Wit M, Watts R K, Estle T L and Schneider J 1969 *J. Phys. Chem. Solids* **30** 963
[29] Chen W M, Monemar B, Gislason H P, Godlewski M and Pistol M E 1988 *Phys. Rev.* B **37** 2558
[30] Spaeth J-M, Niklas J R and Bartram R H 1992 *Structural Analysis of Point Defects in Solids* (Berlin: Springer) p 330
[31] Kita S, Hashimoto M and Iwaizumi M 1982 *J. Magn. Reson.* **46** 361